Granular Matter (2006) 8: 205–220
DOI 10.1007/s10035-006-0009-z

ORIGINAL PAPER

J. Tejchman · A. Niemunis

FE-studies on shear localization in an anistropic micro-polar hypoplastic granular material

Received: 12 August 2005 / Published online: 10 March 2006

Abstract The effect of transverse isotropy on shear localization in cohesionless granular materials is numerically investigated upon monotonous plane strain deformation paths using a hypoplastic constitutive model enhanced by micro-polar terms. In this model, a so-called density function is reformulated and made anisotropic. Dense sand specimens under constant lateral pressure are numerically tested for uniform and stochastic distributions of the initial void ratio and for two different mean grain diameters.

Keywords Anisotropy · Bedding plane · Granular material · Hypoplasticity · Micro-polar theory · Shear zone

1 Introduction

This paper presents several numerical calculations of plane strain compression tests on sand using a hypoplastic constitutive model within a micro-polar (Cosserat) continuum and a novel anisotropic formulation of the dilatancy. It is demonstrated that the anisotropic dilatancy is an important extension which should be considered in numerical simulations of the behaviour of granular materials.

1.1 Anisotropy of the dilatant behaviour

Hypoplastic models for soils [1–8] are inherently isotropic in the sense that material constants do not depend on the choice of the coordinate system. No directions are *initially* distinguished. The rate of stress $\overset{o}{\sigma}_{ij} = E_{ijkl} d_{kl}$ is an incrementally nonlinear function of the rate of deformation d_{ij} because E_{ijk}depends on $d_{ij.}$ too. Due to the dependence of the tangential stiffness $E_{ijkl} = E_{ijkl}(\sigma_{ij}, d_{kl})$ on the current stress tensor σ_{ij}(and not just on the pressure $p = -\sigma_{ii}/3$), the incremental relation is orthotropic with the characteristic directions given by the principal axes of σ_{ij}. However, some granular materials show also an *initial* anisotropy because the stress–strain response depends on the orientation of the major principal stress direction with respect to the bedding plane [9–15]. The initial anisotropy can be observed mainly in the small-strain stiffness and in the dilatancy (defined as $d = d_{ii}/\sqrt{d_{kl} d_{kl}}$ during an isobaric shearing, i.e. at a constant pressure p for a given deviatoric stress rate $\overset{o}{\sigma}{}^{*}_{ij}$, see notation at the end of the paper). The anisotropy of elastic properties at small strains (e.g. $<10^{-4}$) are important for settlement predictions [16]. The anisotropy of dilatant behaviour influences the shear resistance under drained [15] or undrained conditions [17]. The drained strength is understood as the peak value of the stress ratio $(q/p)_{\max}$ whereas the undrained strength, $q_{\max 1} = 2c_u$ (Fig. 1), is understood as an ability to sustain shear stress applied at a constant volume. The undrained behaviour of a granular material under shear deformation is quite important in geotechnical engineering but its constitutive description and physical explanation thereof are not straightforward. The essential phenomenon for the assessment of the soil strength $q_{\max 1}$ during an undrained shearing is the generation of the excess pore water pressure. The dilatancy/contractancy known from isobaric shearing and the pore pressure generation during isochoric shearing are in fact different manifestations of the shear-volumetric coupling. The hypoplastic model used in this paper considers the dilatancy also for stress states below the Coulomb yield surface (contrarily to the classical elasto-plastic models). Its predictions of dilatancy are similar to the ones by Rowe [18]. The dilatancy in sand depends strongly on the history of deformation (so-called historiotropy, [19]) which is present in the arrangement of grains and grain contacts [20]. Two experimental observations seem to speak for implementation of the anisotropy to the dilatant behaviour of the hypoplastic constitutive model:

J. Tejchman (✉)
Faculty for Civil and Environmental Engineering,
Gdansk University of Technology, Gdansk, Poland
E-mail: tejchmk@pg.gda.pl

A. Niemunis
Institute for Soil Mechanics and Foundation Engineering,
Ruhr University of Bochum, Bochum, Germany
E-mail: Andrzej.Niemunis@rub.de

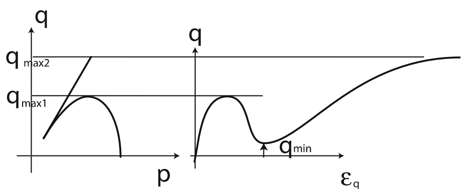

Fig. 1 Isochoric triaxial compression of saturated medium dense and loose sand

(a) During isochoric triaxial compression tests, the characteristic values $q_{\max1}, q_{\min}$ and $q_{\max2}$ (Fig. 1) of the strain-stress curve are much larger than the respective characteristic stresses during the isochoric triaxial extension tests, despite identical initial stresses and void ratios. This effect may be partly attributed to the influence of the third stress invariant and partly to the anisotropic arrangement of grains during the preparation of samples. Our micro-polar (Cosserat) hypoplasticity has been implemented for plane strain only so we defer the discussion of the third stress invariant until the implementation of the Cosserat hypoplastic model is fully three-dimensional.,

(b) Undrained shearing of samples with a larger inclination ($\psi = 90° - \delta$, Fig. 2) of the major principal stress to the normal of the bedding plane leads to significantly larger excess pore pressures [15]. The values of the characteristic stresses $q_{\max1}, q_{\min}$ and $q_{\max2}$ become lower. Similarly in drained tests, the peak strength of $(q/p)_{\max}$ decreases with increasing inclination ψ.

An attempt to explain the anisotropic dependence $q_{\max2}(\psi)$ in the framework of constitutive modelling (assuming that they appear in perfectly homogeneous samples) necessitates an odd assumption that the critical state is anisotropic. A critical state (a residual combination of stress invariants *p,q* and θ and void ratio *e*, [21]) that enables an unconfined plastic flow $d_{ij} \neq 0$ keeping all state variables *p,q*,θ and *e* constant is unlikely to be anisotropic. A unique (or isotropic) critical state line *q (p, θ, e)* is more sensible. A micro-mechanical argument for this uniqueness (or isotropy) is that large shear deformations (e.g. within the shear zone) should completely erase any inherent anisotropy because the initial orientations of grains and their contact normals are completely destroyed. Note that the critical void ratio should be understood locally (for example within a shear zone) and not globally (averaged over the volume of a conventional sample), [22]. We argue that the *differences in strain localization* are responsible for apparent differences in material behaviour observed in *average.* Actually the anisotropy is erased and the critical state is established only within shear zones.

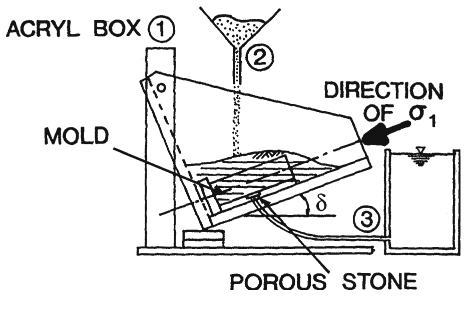

Fig. 2 Method used to prepare a granular specimen [48]

The present modification of the hypoplastic model will describe these effects phenomenologically using an anisotropic density function f_d. Here, we deal with the anisotropy of dilatancy in granular materials under drained conditions only. On one hand, this anisotropy can be treated as an *inherent* property (in section 4, we quantify it) because it is *prescribed* in the process of sedimentation or pluviation which we do not examine here. On the other hand, however, this anisotropy dwindles if large shear deformations are applied. In a well developed shear zone the information about the direction of sedimentation is erased. Since a *decay* of the initial anisotropy due to the shear deformation (in section 4, we propose an evolution equation for this decay) is the only possible evolution described by our model we may speak of a "*strain-reduced*" rather than strain-induced anisotropy.

1.2 Constitutive modelling

In continuum approach to granulate mechanics, numerous elasto-plastic [23–25] and hypoplastic models [1–6,26–28] have been developed. In order to describe properly the shear zone formation (thickness, inclination and spacing), these approaches have to be enriched by a characteristic length of microstructure by means of a micro-polar [7,8,29–33], non-local [7,8,34,35], second-gradient theory [7,8,36–38] and viscosity [39,40]. Due to the presence of a characteristic length of micro-structure (connected to a mean grain diameter), these approaches regularize the solution, i.e. they preserve the well-posedness of the boundary value problem (BVP) especially during softening and localization [41]. Objective and properly convergent numerical solutions for localized deformation (mesh-insensitive load-displacement diagram and mesh-insensitive deformation pattern) are achieved. The solutions are independent of discretization provided the elements are sufficiently small (of size of several grain diameters). Other numerical technique which also enables to remedy the drawbacks of a standard FE-method and to obtain mesh-independent results during the description of the formation of shear zones is a strong discontinuity approach allowing a finite element with a displacement discontinuity [42,43].

As already mentioned, the *averaged* change of volume and the *averaged* residual state may be strongly influenced by strain localization [18,44] in a granular specimen. Therefore, a Cosserat continuum is of importance in this study. Using the micro-polar (Cosserat) continuum, an apparent anisotropy of the residual state (of averaged quantities) can be explained preserving the concept of the isotropic (or unique) critical state in the framework of the material model. Apart from the isochoric values $q_{\max1}$ and $q_{\max2}$, the anisotropic dilatancy influences the drained (isobaric) stress-strain behaviour

[45–50]. The stiffness and the peak friction angle are higher for less inclined loading and the angle of the shear zone with respect to the bottom becomes larger [48]. For large monotonic shearing, the residual stress is not affected by the initial anisotropy [48,50].

In hypoplasticity, two descriptions of the inherent anisotropy have been proposed. The first one was suggested by Bauer et al. [51] and it is based on an earlier work by Wu [52]. Bauer et al. [51] have introduced an additional structure tensor which takes into account the space orientation of the bedding plane. Their concept follows actually the idea of Boehler and Sawczuk [9] proposed for elasto-plasticity. The structural term affects only the nonlinear part of the hypoplastic equation and vanishes at the critical state. Such tensorial expression modifies the yield surface, increasing $(q/p)_{\max}$ for the major principal stress perpendicular to the bedding plane. It also renders the flow rule more dilatant (d becomes larger), although it is not clear in what extend this effect is due to the modified flow rule and what is the contribution of the increased value of $(q/p)_{\max}$ (for higher stress ratios the all hypoplastic models predict larger d). Examples in [51] refer only to compression tests of *dense* sand. For dense sands $q_{\max 1}$ and $q_{\min}$ do not exist because the curve $q(\epsilon)$ monotonously increases. Actually, the anisotropy of dilatancy in medium dense and loose sand is much more important. The anisotropic model in [51] introduces 3 additional material parameters (without a clear physical meaning) but only two of them are tested. This model is unable to describe an anisotropy if the initial void ratio of granulates is equal to the critical void ratio $e_c(p)$.

In the present paper, an alternative implementation of anisotropy is used. It is based on a simpler idea by Niemunis [53]. Only a scalar density function f_d is made dependent on the orientation of the major principal stress to the bedding plane. The tensorial constitutive functions are left unchanged. Also the critical state defined by functions $e(p)$ and $q(p,\theta)$ remain isotropic. The anisotropy of f_d may be erased by shear deformation, although a substantial strain path length is required. The description of the anisotropy and its evolution are presented in detail in section 4. Similarly as in the model by Bauer et al. [51], the strength $(q/p)_{\max}$ and the dilatancy become larger if the inclination ($\psi = 90° - \delta$, Fig. 2) of the major principal stress to the normal of the bedding plane becomes smaller. No additional modifications of the flow rule are postulated. Similarly as in [51], the anisotropy affects the peak strength but not the critical state line (CSL) which remains unique and isotropic. Apart from being simpler, the formulation in [53] works for all densities. Both approaches [51] and [53] perform rather poorly upon unloading [15] so one may consider to include the direction of stretching in the density factor in future.

As already mentioned in section 1.1, the measurements of dilatancy may be blurred by the omnipresent shear localization. Therefore, a spontaneous shear zone formation in sand during plane strain compression under constant lateral pressure will be numerically investigated with the finite element method and a micro-polar hypoplastic constitutive model [9, 33] which is able to describe the essential properties of granular bodies during shear localization in a wide range of pressures and densities during monotonous deformation paths. In the FE-analyses, a uniform and stochastic distribution of the initial void ratio was assumed. The height of a finite element was not larger than five times mean grain diameter to properly capture shear localization [7,8,31]. The effect of transverse isotropy on shear localization in cohesionless granular materials during plane strain compression has not been numerically investigated within enhanced hypoplasticity yet.

2 Experiments by Tatsuoka et al. [48]

Comprehensive laboratory experiments on the effect of textural anisotropy (fabric) were performed for plane strain compression by Tatsuoka et al. [48]. The tests were carried out mainly with Silver Leighton Buzzard sand composed of subround grains (mean grain diameter $d_{50} = 0.62$ mm, nonconformity coefficient $U_c = 1.11$). The specimen was 20 cm long and 8 cm wide. The confining platens were very smooth. Dense specimens were prepared. Several different angles δ were employed between the pouring direction and the direction of the major principal stress (Fig. 2). The specimen was wetted, frozen, thawed and re-dried. Figure 3 presents the relationships among the stress ratio σ_1/σ_3, the average shear strain $\gamma = \epsilon_1 - \epsilon_3$ and the average volumetric strain $\epsilon_v = \epsilon_1 + \epsilon_3$ for different angles of δ between 90° and 0° at $\sigma_3 = 80$ kPa (for dense SLB sand with $e_0 = 0.555$–0.563).

The peak internal friction angle calculated by the Mohr's formula with the aid of principle stresses increases with

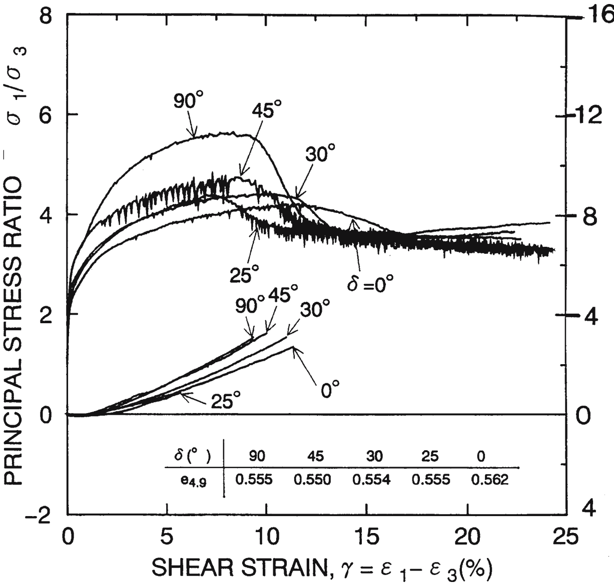

Fig. 3 Relationships among the stress ratio σ_1/σ_3, the average shear strain $\gamma = \epsilon_1 - \epsilon_3$ and the average volumetric strain $\epsilon_v = \epsilon_1 + \epsilon_3$ for different angles of δ between 90 and 0 degrees at $\sigma_3 = 80$ kPa [48] ($\psi = 90° - \delta$)

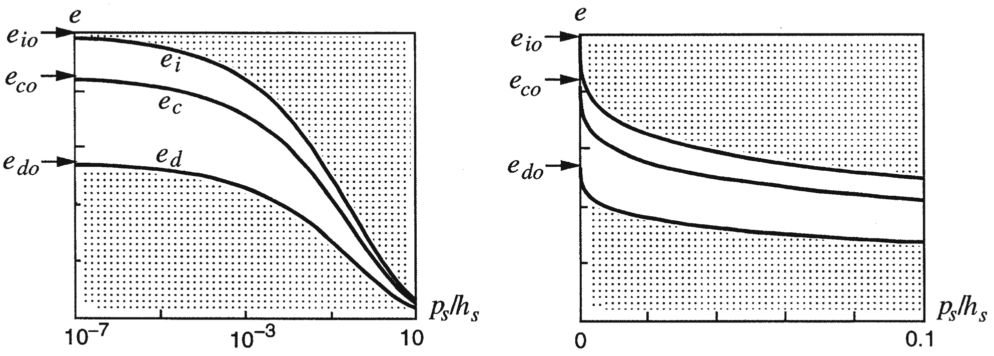

Fig. 4 Relationship between void ratios e_i, e_c and e_d and mean pressure p_s in a semi-logarithmic (**a**) and linear (**b**) scale (*gray zones* denote inadmissible states)

decreasing angle $\psi = 90° - \delta$, and is: $\phi_p = 39.6°$ ($\psi = 90°$), $\phi_p = 40.0°$ ($\psi = 65°$), $\phi_p = 42.0°$ ($\psi = 45°$), $\phi_p = 43.9°$ ($\psi = 25°$) and $\phi_p = 45.1°$ ($\psi = 0°$), respectively. Thus, the peak friction angle can decrease by about 10% with decreasing ψ. The peak internal friction angle was reached for the shear strain $\gamma = 6$–10% (which decreased as ψ increased, in particular for $\psi > 45°$). The residual internal friction angle was about 24°–25.5°. The average volumetric strain was the largest for $\psi = 0°$, and later for $\psi = 45°$, $\psi = 60°$, $\psi = 90°$, and $\psi = 65°$, respectively (Fig. 3).

3 Isotropic micro-polar hypoplastic model for plane strain

The hypoplastic constitutive models [1–8] can predict the onset of shear localization. However, they cannot describe realistically shear localization in a post-peak regime since they do not incorporate a characteristic length of microstructure. In this paper, a micro-polar theory was taken advantage of to introduce a characteristic length [8]. A micro-polar model has good physical grounds since it takes into account Cosserat rotations (resultant grain rotations from a certain region of the granular specimen) and couple stresses which are significant during shearing [54,55]. Its other advantages are: the characteristic length is directly related to the mean grain diameter [7,8] and realistic wall boundary conditions at the interface of granulate with a structure (with consideration of the wall roughness) can be derived [56]. Pasternak and Mühlhaus [57] have demonstrated that the additional rotational degree of freedom of a Cosserat continuum arises naturally by mathematical homogenization of an originally discrete system of spherical grains with contact forces and contact moments. The Cosserat model is only suitable for shear dominated problems but not for tension dominated applications [40,41].

The present micro-polar hypoplastic constitutive law has been formulated by extending a hypoplastic model by Gudehus [3] and Bauer [4] by means of a micro-polar continuum [29] which takes into account two linked kinds of deformation: micro-rotation at the particle scale and macro-deformation at the structural scale. Each material point has for the case of plane strain three degrees of freedom: two translations u_i and one independent rotation ω^c (Fig. 5a). Deformation is described by the following six quantities:

$$\varepsilon_{11} = u_{1,1}, \quad \varepsilon_{22} = u_{2,2}, \tag{1}$$

$$\varepsilon_{12} = u_{1,2} + \omega^c, \quad \varepsilon_{12} = u_{1,2} + \omega^c, \tag{2}$$

$$\kappa_1 = \omega^c_{,1}, \quad \kappa_1 = \omega^c_{,1} \tag{3}$$

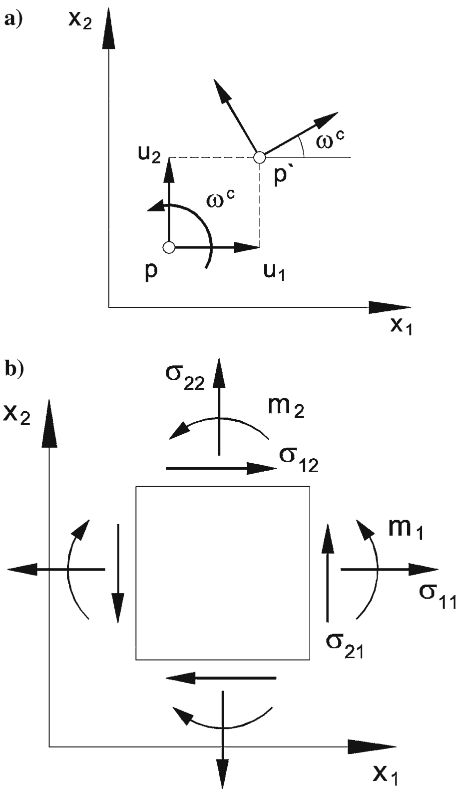

Fig. 5 Plane strain Cosserat continuum: **a** degrees of freedom (u_1 horizontal displacement, u_2 vertical displacement, ω^c Cosserat rotation), **b** stresses σ_{ij} and couple stresses m_i at an element

Force and moment equilibrium (Fig. 5b) require (static case) that

$$\sigma_{11,1}+\sigma_{12,2}-f_1^B=0, \tag{4}$$

$$\sigma_{21,1}+\sigma_{22,2}-f_2^B=0, \tag{5}$$

$$m_{1,1}+m_{2,2}+\sigma_{21}-\sigma_{12}-m^B=0, \tag{6}$$

where f_i^B and m^B are the volume body forces and volume body moment, respectively. Eqs. 4–6 are equivalent to the virtual work principle

$$\int_B (\sigma_{ij}\delta\varepsilon_{ij}+m_i\delta\kappa_i)\mathrm{d}V=\int_B (f_i^B\delta u_i+m^B\delta\omega^{\mathrm{c}})\mathrm{d}V + \int_{\partial_1 B} t_i\delta u_i \mathrm{d}A+\int_{\partial_1 B} m\delta\omega^c \mathrm{d}A, \tag{7}$$

wherein $t_i=\sigma_{ij}n_j$ and $m=m_i n_i$, and t_i and m are prescribed boundary tractions and moment on the boundary $\partial_1 B$ with the normal vector n_i. $\delta\epsilon_{ij}$ and $\delta\kappa_i$ denote virtual strains and curvatures, respectively, δu_i are virtual displacements, $\delta\omega^{\mathrm{c}}$ is the virtual Cosserat rotation, A is the surface and V denotes the volume. Virtual displacements and Cosserat rotation vanish on those parts of the boundary where kinematic boundary conditions are prescribed. The virtual work principle (equation 7) is used to formulate the FE-equations of motion in a micro-polar continuum [29].

The polar extension of the hypoplastic constitutive law [3,4] has been formulated analogously to Mühlhaus' formulation [29] of plasticity (for details, the reader is referred to [31]). A micro-polar hypoplastic constitutive law describes the stress rate and couple stress rate depending on the current void ratio e, stress σ_{ij} and couple stress m_i and rate of deformation d_{ij} and curvatures k_i. Due to the incremental non-linearity with respect to the rate of deformation and curvature, it is able to describe both a non-linear stress-strain and volumetric behaviour of granular bodies during shearing up to and after the peak with two single tensorial equations. It includes also: barotropy (dependence on pressure level), pycnotropy (dependence on density), dilatancy and contractancy and a characteristic length of micro-structure. In contrast to elasto-plastic models, a decomposition of deformation and curvatures components into elastic and plastic parts, an explicit formulation of a yield surface, plastic potential, flow rule and hardening rule is not needed. The constitutive law can be summarized for plane strain as follows [8,31]:

$$\overset{o}{\sigma}_{ij}=f_s[L_{ij}(\hat{\sigma}_{kl},\hat{m}_k,d_{kl}^{\mathrm{c}},k_k d_{50}) + f_d N_{ij}(\hat{\sigma}_{ij})\sqrt{d_{kl}^{\mathrm{c}}d_{kl}^{\mathrm{c}}+k_k k_k d_{50}^2}], \tag{8}$$

$$\overset{o}{m}_i/d_{50}=f_s[L_i^{\mathrm{c}}(\hat{\sigma}_{kl},\hat{m}_k,d_{kl}^{\mathrm{c}},k_k d_{50}) + f_d N_i^{\mathrm{c}}(\hat{m}_i)\sqrt{d_{kl}^{\mathrm{c}}d_{kl}^{\mathrm{c}}+k_k k_k d_{50}^2}], \tag{9}$$

$$L_{ij}=a_1^2 d_{ij}^{\mathrm{c}}+\hat{\sigma}_{ij}(\hat{\sigma}_{kl}d_{kl}^{\mathrm{c}}+\hat{m}_k k_k d_{50}), \tag{10}$$

$$L_i^{\mathrm{c}}=a_1^2 k_i d_{50}+a_1^2\hat{m}_i(\hat{\sigma}_{kl}d_{kl}^{\mathrm{c}}+\hat{m}_k k_k d_{50}), \tag{11}$$

$$N_{ij}=a_1(\hat{\sigma}_{ij}+\hat{\sigma}_{ij}^*), \tag{12}$$

$$N_i^{\mathrm{c}}=a_1^2 a_c\hat{m}_i, \tag{13}$$

$$\hat{\sigma}_{ij}=\frac{\sigma_{ij}}{\sigma_{kk}}, \tag{14}$$

$$\hat{m}_i=\frac{m_i}{\sigma_{kk}d_{50}}, \tag{15}$$

$$\overset{o}{\sigma}_{ij}=\dot{\sigma}_{ij}-w_{ik}\sigma_{kj}+\sigma_{ik}w_{kj}. \tag{16}$$

$$\overset{o}{m}_i=\dot{m}_i-0.5w_{ik}m_k+0.5m_k w_{ki}, \tag{17}$$

$$d_{ij}=\frac{(v_{i,j}+v_{j,i})}{2},\quad w_{ij}=\frac{(v_{i,j}-v_{j,i})}{2}, \tag{18}$$

$$d_{ij}^{\mathrm{c}}=d_{ij}+w_{ij}-w_{ij}^{\mathrm{c}},\ k_i=w_{,i}^{\mathrm{c}}, \tag{19}$$

$$w_{kk}^{\mathrm{c}}=0,w_{21}^{\mathrm{c}}=-w_{12}^{\mathrm{c}}=w^{\mathrm{c}}, \tag{20}$$

$$\dot{e}=(1+e)d_{kk}, \tag{21}$$

$$e_i=e_{i0}\exp[-(-\sigma_{kk}/h_s)^n], \tag{22}$$

$$e_d=e_{d0}\exp[-(-\sigma_{kk}/h_s)^n], \tag{23}$$

$$e_c=e_{c0}\exp[-(-\sigma_{kk}/h_s)^n], \tag{24}$$

$$f_s=\frac{h_s}{nh_i}\left(\frac{1+e_i}{e_i}\right)\left(\frac{e_i}{e}\right)^\beta\left(-\frac{\sigma_{kk}}{h_s}\right)^{1-n}, \tag{25}$$

$$h_i=\frac{1}{c_1^2}+\frac{1}{3}-\left(\frac{e_{i0}-e_{d0}}{e_{c0}-e_{d0}}\right)^\alpha\frac{1}{c_1\sqrt{3}}, \tag{26}$$

$$f_d=\left(\frac{e-e_d}{e_c-e_d}\right)^\alpha, \tag{27}$$

$$1/a_1=c_1+c_2\sqrt{\hat{\sigma}_{kl}^*\hat{\sigma}_{kl}^*}[1+\cos(3\theta)], \tag{28}$$

$$\cos(3\theta)=-\frac{\sqrt{6}}{[\hat{\sigma}_{kl}^*\hat{\sigma}_{kl}^*]^{1.5}}(\hat{\sigma}_{kl}^*\hat{\sigma}_{lm}^*\hat{\sigma}_{mk}^*), \tag{29}$$

$$c_1=\sqrt{\frac{3}{8}}\frac{(3-\sin\phi_c)}{\sin\phi_c},c_2=\frac{3}{8}\frac{(3+\sin\phi_c)}{\sin\phi_c}. \tag{30}$$

The characteristic void ratios e_i, e_d and e_c decrease with the pressure $p=-\sigma_{kk}/3$ according to the exponential functions (equations 22,23,24) shown in Fig. 4. The parameter a_1 is equal to 0.25–0.33 for the usual critical friction angles of granulates [31]. The remaining parameters are adopted from the non-polar version of hypoplasticity. The constitutive relationship requires the following ten material constants: e_{i0}, e_{d0}, e_{c0}, ϕ_c, h_s, β, n, α, a_c and d_{50}. An exact calibration procedure of first 8 constant was given by Herle and Gudehus [58]. The parameters h_s and n are estimated from a single oedometric compression test with an initially loose specimen (h_s reflects the slope of the curve in a semi-logarithmic representation, and n its curvature). The constants α and β are found from a triaxial or plane strain test with a dense specimen and trigger the magnitude and position of the peak friction angle. The angle ϕ_c is determined from the angle of repose or measured in a triaxial test with a loose specimen. The values of e_{i0}, e_{d0}, e_{c0} and d_{50} are obtained with conventional index tests ($e_{c0}\approx e_{\max}$, $e_{d0}\approx e_{\min}$, $e_{i0}\approx(1.1–1.5)\ e_{\max}$). A micro-polar parameter a_c can be correlated with the grain roughness with the aid of a numerical analysis for

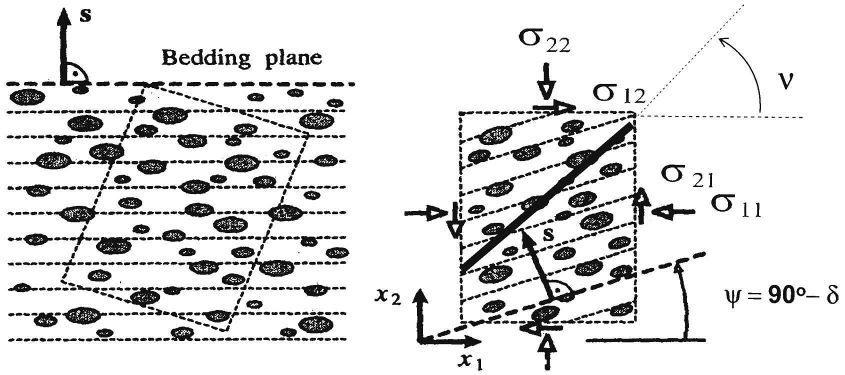

Fig. 6 Normal vector $\boldsymbol{s}$ of the bedding plane (**a**) and its inclination ψ (**b**) with respect to a fixed co-ordinate system (ψ bedding plane inclination, υ shear zone inclination against the bottom) ($\psi = 90° - \delta$)

shearing of a narrow granular strip between two very rough boundaries [38]. It can be connected to the parameter a_1 (e.g. $a_c = 1.0/a_1$). In this case, the function $N_i^c = a_1 \hat{m}_i$ (Eq. 13).

4 Anisotropic formulation of f_d

In the basic hypoplastic model, the density factor f_d (a function of void ratio e and pressure p, equations 22,23,24,27) is supposed to influence the shear resistance at peak. At large stress ratios q/p, the flow rule may be dilatant ($d > 0$ for $\dot{q} > 0$) or contractant ($d < 0$ for $\dot{q} < 0$). At smaller stress ratios q/p, the flow rule is always contractant. Smaller factors f_d allow for the larger stress ratios q/p and this increases the dilatancy. In the hitherto existing versions of hypoplasticity [3–6], f_d was a function of void ratio and pressure alone (hence it was an isotropic function). Due to the experimental observations (section 2) showing that the shear resistance at peak and dilatancy depend also upon the direction of grain sedimentation, f_d is proposed to be an anisotropic function [53]

$$f_d = \left(\frac{e - e_d}{e_c - e_d}\right)^{\alpha} \tag{31}$$

with

$$e_c = \bar{e}_{c0} \exp[-(-\sigma_{kk}/h_s)^n] \tag{32}$$

and

$$\bar{e}_{c0} = e_{c0} + \Delta e_{c0} \vec{M}_{ij} \hat{\sigma}^*_{ij} \tag{33}$$

The normalized deviator $\hat{\sigma}^*_{ij} = \sigma^*_{ij}/\sigma_{kk}$ is multiplied by the unit dyadic tensor

$$\vec{M}_{ij} = \frac{M_{ij}}{\sqrt{M_{kl}M_{kl}}}, \quad \text{wherein } M_{ij} = s_i s_j, \tag{34}$$

in which $\boldsymbol{s}$ denotes a unit vector normal to the bedding plane; $\boldsymbol{s} = [-\sin\psi, \cos\psi, 0]$ (Fig. 6). The components M_{ij} written in the matrix form are

$$\begin{bmatrix} \sin^2\psi & -\sin\psi\cos\psi & 0 \\ -\sin\psi\cos\psi & \cos^2\psi & 0 \\ 0 & 0 & 0 \end{bmatrix}. \tag{35}$$

Evidently, the novel $\bar{e}_{c0}$ takes into account the inclination of the deviatoric stress to the bedding plane. The parameter Δe_{c0} describes the anisotropic discrepancy of the critical void ratio e_{c0} from the isotropic reference value at $p = 0$. This discrepancy is subject to a decay depending on the deformation as shown in equation (36). Assuming that anisotropic effects vanish for large deformations [62], $\bar{e}_{c0} \to e_{c0}$ (hence $\Delta e_{c0} \to 0$), the decay of Δe_{c0} is proposed in a simple form

$$\Delta\dot{e}_{c0} = -\Delta e_{c0} B \sqrt{d^c_{ij} d^c_{ij} + k_i k_i d_{50}^2} \tag{36}$$

The *initial* value of Δe_{c0} at $t = 0$ and the rate of decay B (the only additional material constant) must be found by curve fitting until some empirical correlations are established (as it was done by Herle and Gudehus [58] for the remaining hypoplastic material constants). The initial value of $\Delta e_{c0} \vec{M}_{ij} \hat{\sigma}^*_{ij}$ cannot be obviously larger than $(e_{c0} - e_{d0})$ or $(e_{i0} - e_{c0})$ for any possible stress. The evolution equation for Δe_{c0} (equation 36) is objective since d^c_{ij} and k_i are objective [29].

5 FE-calculations

The FE-analyses were carried out with the material constants for so-called Karlsruhe sand: $e_{i0} = 1.30$, $e_{d0} = 0.51$, $e_{c0} = 0.82$, $\phi_c = 30°$, $h_s = 190\,\mathrm{MPa}$, $\beta = 1$, $n = 0.40$, $\alpha = 0.20$, $a_c = 1.0 \times a_1^{-1}$ and $d_{50} = 0.5\,\mathrm{mm}$ [4]. In turn, the anizotropic constants were assumed to be $\Delta e_{c0}(t = 0) = 0.25$ and $B = 5$. The difference between the peak internal friction angles at $\psi = 0°$ and $\psi = 90°$ is about 10% (Fig. 7). The confining pressure was chosen as $\sigma_{conf} = 200\,\mathrm{kPa}$. The initial void ratio of the dense sand specimen was assumed to be $e_0 = 0.60$.

Figure 7 shows the results of element tests with a non-polar hypoplastic model demonstrating the effect of the direction of the bedding plane on the evolution of the vertical normal stress $\sigma_{22} = P/(\sigma_c bl)$ and void ratio e during plane strain compression in an initially dense specimen. In the element tests, the vertical normal strain $\epsilon_{22} = u_2/h$ was prescribed.

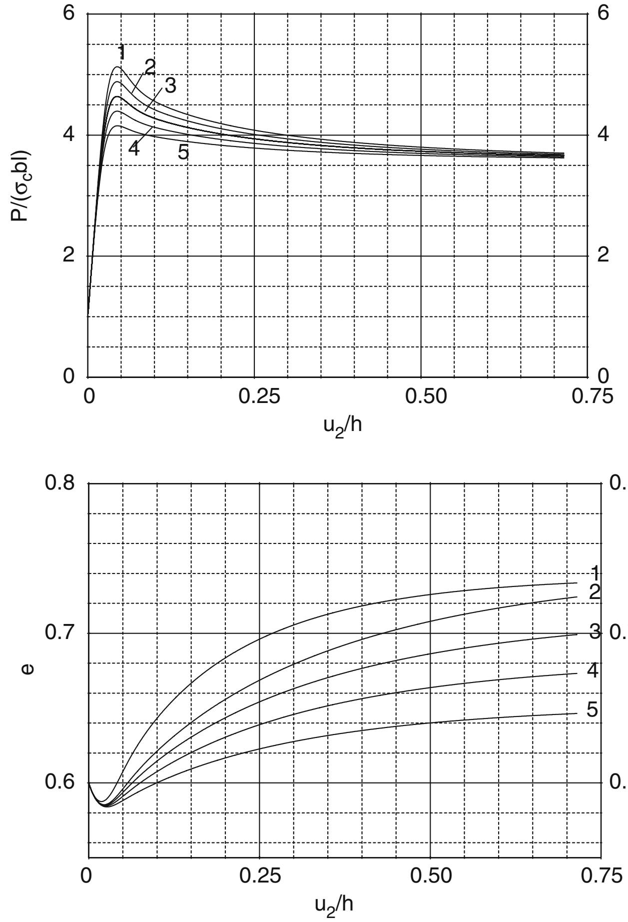

Fig. 7 Plane strain compression test (element test): effect of the bedding plane inclination ψ of Fig. 6 on the normalized load-displacement curve and void ratio evolution ($e_o = 0.60$, $\Delta e_{c0}(t = 0) = 0.25$, $B = 5$): *1* $\psi = 0°$, *2* $\psi = 30°$, *3* $\psi = 45°$, *4* $\psi = 60°$, *5* $\psi = 90°$

The influence of $\Delta e_{c0}(t = 0)$ on the curve σ–ϵ in the element test is presented in Fig. 8.

The larger the bedding angle ψ (Fig. 6) the smaller the maximum vertical stress in the specimen and void ratio changes. The residual vertical force is the same independently of ψ. However, in contrast with experiments, the strain corresponding to the maximum vertical force is similar. The effect of anisotropy increases with increasing $\Delta e_{c0}(t = 0)$. The larger the parameter $\Delta e_{c0}(t = 0)$, the higher the internal friction angles at peak and at residual state. The shear stresses are very small (however, they occur due to anisotropy). In contrast to laboratory tests, the shear strain corresponding to the peak internal friction angle does not change with bedding angle. The peak overall internal friction angle calculated with the aid of averaged principle stresses $\sigma_1 = P/(bl)$ (vertical dead load) and $\sigma_2 = \sigma_{\mathrm{conf}}$ (following lateral load)

$$\phi_m = \arcsin \frac{\sigma_1 - \sigma_2}{\sigma_1 + \sigma_2} \tag{37}$$

changes between 37.7 (for $\psi = 90°$) and 42.4° (for $\psi = 0°$). The residual friction angle is about 34.7°. The critical void ratio lies between 0.65 (for $\psi = 90°$) and 0.73 (for

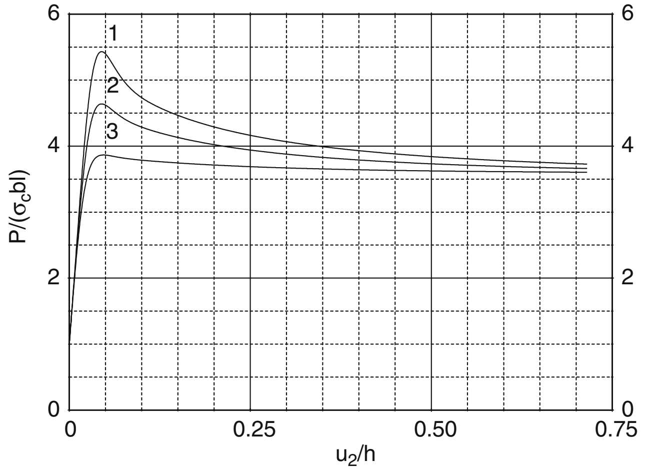

Fig. 8 Plane strain compression test (element test): effect of the bedding plane inclination ψ of Fig. 6 on the normalized load-displacement curve ($e_o = 0.60$, $\Delta e_{c0}(t = 0) = 0.40$, $B = 5$): *1* $\psi = 0°$, *2* $\psi = 45°$, *3* $\psi = 90°$

$\psi = 0°$). A large vertical normal strain is needed to approach a residual state ($u_2/h = 0.75\%$).

FE-calculations of plane strain compression tests were performed with a sand specimen which was $h = 14$ cm high and $b = 4$ cm wide [8] (similarly as in the experiments by Vardoulakis [59] with Karlsruhe sand). In total, 896 quadrilateral elements ($0.25 \times 0.25\,\mathrm{cm}^2$) divided into 3,584 triangular elements were used to avoid volumetric locking. The integration was performed with one sampling point placed in the middle of each element.

A static deformation in sand was imposed through a constant vertical displacement increment Δu prescribed at nodes along the upper edge of the specimen. The boundary conditions of the sand specimen implied no shear stress at the smooth top and smooth bottom. To preserve the stability of

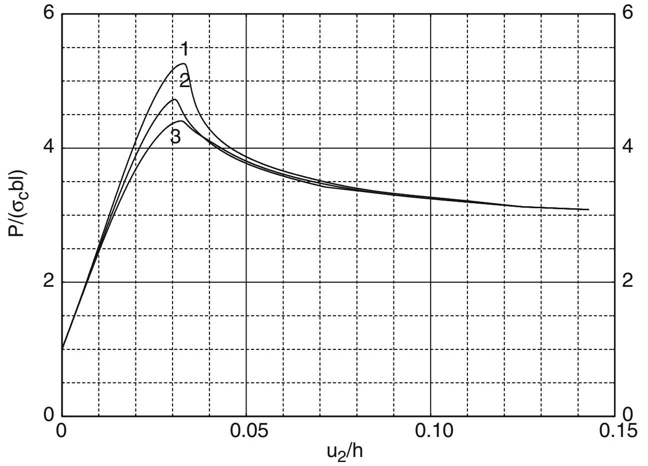

Fig. 9 Effect of the bedding plane inclination ψ of Fig. 6 on the normalized load-displacement curve (stochastic distribution of $e_o = 0.60$, $d_{50} = 0.5$ mm, $\Delta e_{c0}(t = 0) = 0.25$, $B = 5$): *1* $\psi = 0°$, *2* $\psi = 45°$, *3* $\psi = 90°$

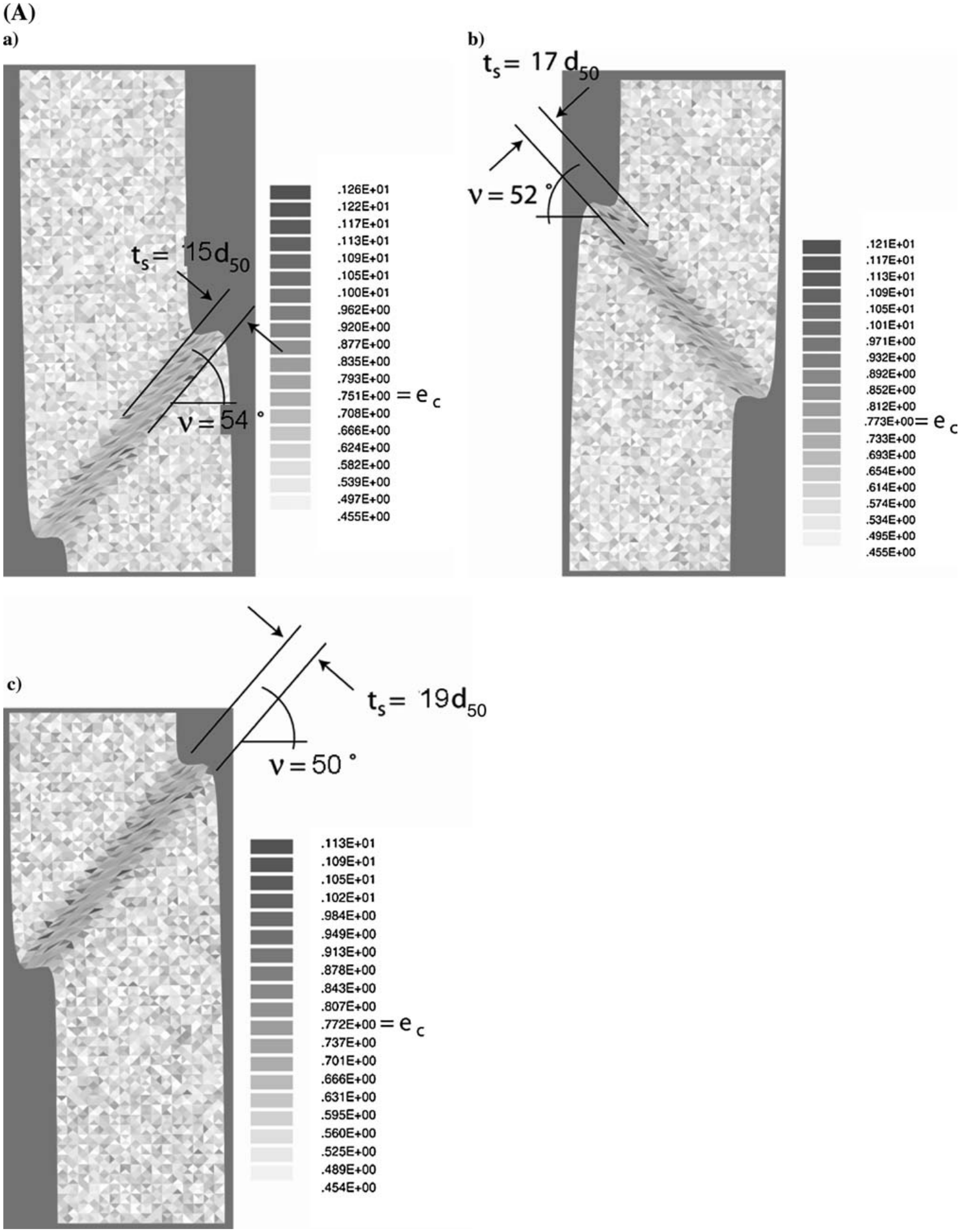

Fig. 10 Deformed specimen with the distribution of void ratio e (**A**) and strain measure $\bar{\varepsilon} = \sqrt{\varepsilon_{ij}\varepsilon_{ij}}$ (**B**) at residual state (stochastic distribution of $e_0 = 0.60$, $d_{50} = 0.5\,\text{mm}$, $\Delta e_{c0}(t = 0) = 0.25$, $B = 5$): **a** $\psi = 0°$, **b** $\psi = 45°$, **c** $\psi = 90°$

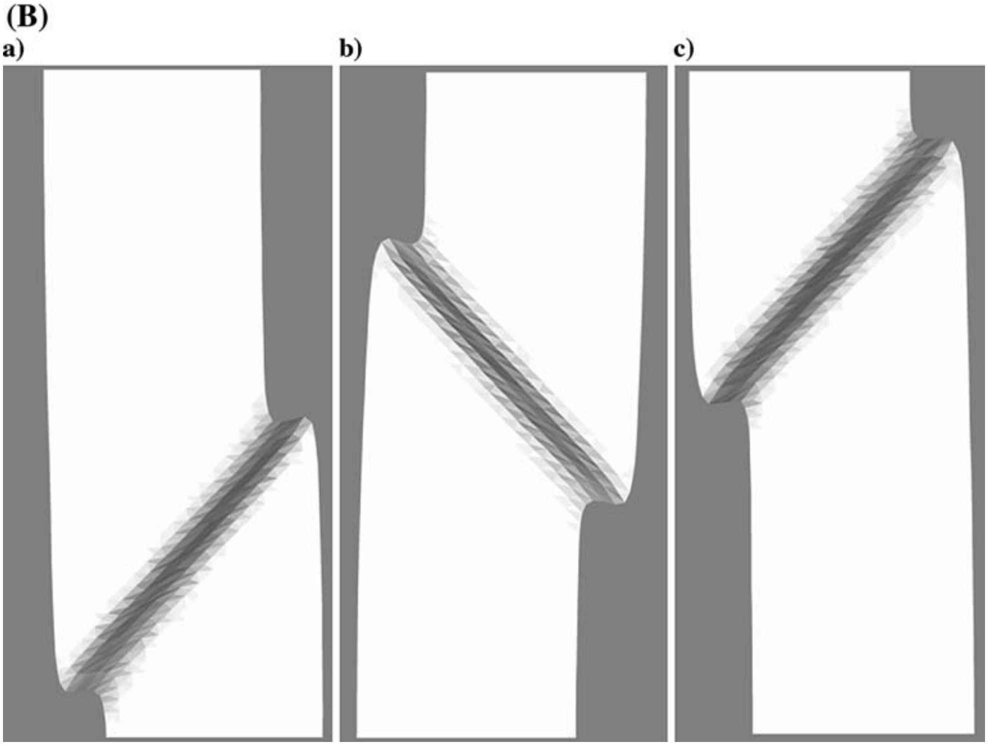

Fig. 10 (Contd.)

the specimen against horizontal sliding along the top boundary, the node in the middle of the top edge was kept fixed. The vertical displacement increments were chosen as $\Delta u/h = 0.00005$ (8,000 steps were performed).

In spite of the presence of anisotropy, the same initial stress state was assumed for the different bedding angles ψ. $\sigma_{22} = \gamma_d x_2$ and $\sigma_{11} = \sigma_{33} = K_o \gamma_d x_2$, $\sigma_{12} = \sigma_{21} = 0$, $m_1 = m_2 = 0$ ($K_o = 0.45$ [4]). Next, the confining pressure of σ_{conf}=200 kPa was prescribed to the specimen. The initial calculations indicated an insignificant effect of the initial stress state on FE-results.

The calculations were carried out with an uniform initial void ratio or with a spatially uncorrelated stochastic distribution following [60,61]. In the latter case, the spatially fluctuating initial void ratio e_o was calculated for individual finite elements (or Gauss integration points) from the formula given by

$$e_o = -\frac{1}{\lambda} \ln[(1-r)\exp(-\lambda e_m) + r\exp(-\lambda e_M)], \quad (38)$$

wherein the parameters are: $\lambda = 1.0$ (for a mean void ratio $e_0 = 0.60$), $e_m = 0.001$ and $e_M = 1.641$ [61]. The random number r is chosen between 0 and 1. Equation (36) has been derived analogously to the partition function of statistical mechanics, however imposing bounds e_m and e_M upon the size of the individual Voronoi cells. The deviation of the distribution of void ratio increases with decreasing number of voids (grains) in a volume element and decreasing mean global void ratio of the specimen. Since the area of each finite element was $5\,d_{50} \times 5d_{50}$, the initial void ratio in each element was assumed as the mean value of 25 random values calculated by Equation (36) (i.e. as if the thickness of the model was d_{50}).

For the solution of a non-linear system, a modified Newton–Raphson scheme with line search was used with a global stiffness matrix calculated with only first terms of the constitutive equations (equations 5 and 6). The stiffness matrix was updated every 100 steps. To accelerate the calculations in the softening regime, the initial increments of displacements and Cosserat rotations in each calculation step were assumed to be equal to the final increments in the previous step. The procedure was found to yield a sufficiently accurate and fast convergence. The magnitude of the maximum out-of-balance force at the end of each calculation step (in the softening regime) smaller than 2% of the calculated total vertical force along the top of the granular specimen was considered negligible and stopped the equilibrium iteration. Due to the presence of non-linear terms taking into the direction of the deformation rate and material softening, this procedure turned out to be more efficient than the full Newton–Raphson method. The iteration steps were performed using translational and rotational convergence criteria. For the time integration of stresses in finite elements, a one-step Euler forward scheme was applied.

The calculations were carried out only with large deformations and curvatures using the so-called "Updated Lagrangian" formulation due to their effect on the results [8]. In the calculations, the actual configuration and volume of finite elements was taken into account.

5.1 Stochastic distribution of the initial void ratio

The FE-results for different bedding plane orientations ψ (0°, 45° and 90°) with a stochastic distribution of the initial void ratio with the mean value equal to 0.60 are depicted in Figs. 9, 10, 11. The normalized load-displacement curves are shown in Fig. 9. In turn, Fig. 10 shows the deformed FE-meshes with the distribution of the void ratio e and strain measure assumed as $\bar{\varepsilon} = \sqrt{\varepsilon_{ij}\varepsilon_{ij}}$ (equations 1 and 2) at residual state ($u_2/h = 0.10$). The deformed FE-meshes with the distribution of the strain measure before and after the peak are depicted in Fig. 12. The darker the region, the higher e and $\bar{\varepsilon}$. The entire range of the void ratio e and strain measure $\bar{\varepsilon}$ was divided into 20 different shades of grey.

The maximum and residual vertical force on the top is the largest (similarly as in experiments, Fig. 3) for the bedding angle of $\psi = 0°$ and the smallest for $\psi = 90°$ (Fig. 10). The peak friction angles vary between 42.9° ($\psi = 0°$) and 39.0° ($\psi = 90°$), respectively. The residual internal friction angles, 31.5–31.7°, are similar. The results are qualitatively in agreement with DEM simulations [21]. The shear strain corresponding to the peak is the largest for $\psi = 0°$ and the smallest for $\psi = 45°$.

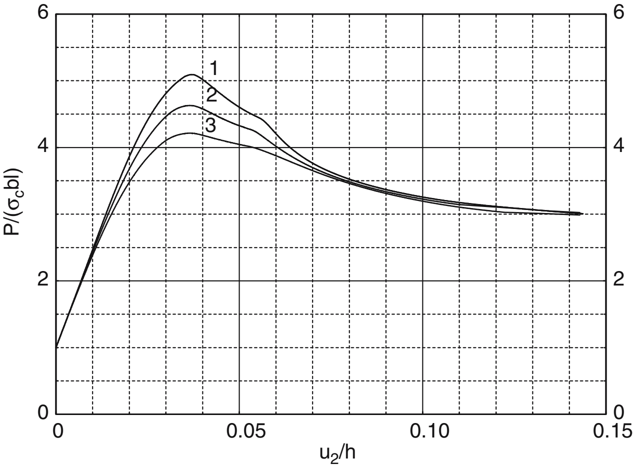

Fig. 12 Effect of the bedding plane inclination θ of Fig. 6 on the normalized load-displacement curve (uniform distribution of $e_0 = 0.60$, $d_{50} = 0.5\,\text{mm}$, $\Delta e_{c0}(t = 0) = 0.25$, $B = 5$): *1* $\psi = 0°$, *2* $\psi = 45°$, *3* $\psi = 90°$

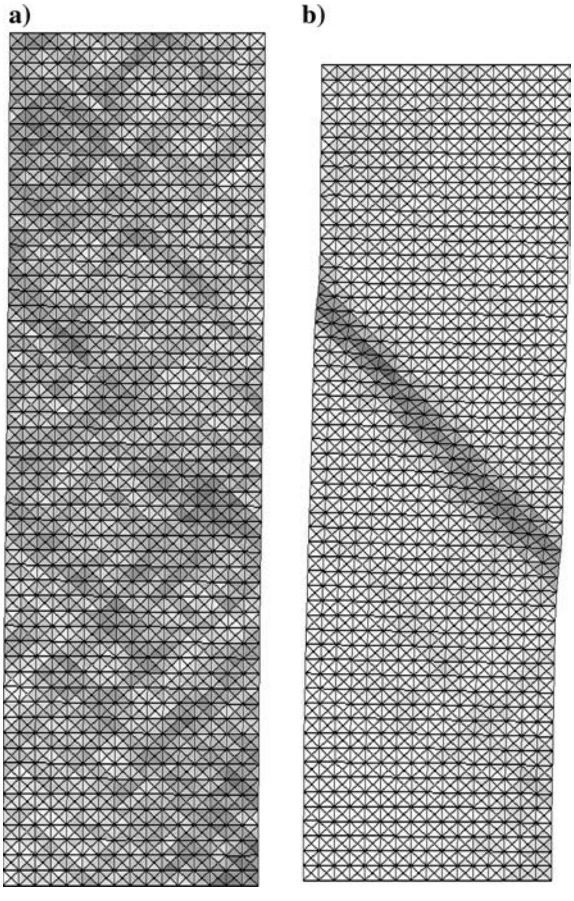

Fig. 11 FE-mesh with distribution of strain measure $\bar{\varepsilon} = \sqrt{\varepsilon_{ij}\varepsilon_{ij}}$ at different vertical deformations: **a** u_2/h=0.027, **b** u_2/h=0.036 (stochastic distribution of $e_0 = 0.60$, $d_{50} = 0.5\,\text{mm}$, $\Delta e_{c0}(t = 0) = 0.25$, $B = 5$, $\theta = 45°$)

One shear zone occurs inside of the specimen which crosses the specimen and whose location is induced by a stochastic distribution of the initial void ratio. The thickness on the basis of shear deformation and strain measure $\bar{\varepsilon}$ (Fig. 10b) increases from about $t_s = 7.5\,\text{mm}$ ($15 \times d_{50}$) for $\psi = 0°$ up to $t_s = 9.5\,\text{mm}$ ($19 \times d_{50}$) for$\psi = 90°$, respectively. Due to the lack of the experimental data, this outcome cannot be compared with experiments. In turn, the inclination against the bottom decreases from about $\nu = 54°$ ($\psi = 0°$) down to $\nu = 50°$ ($\psi = 90°$). In the experiments [49], a more significant decrease of the shear zone inclination was however observed (from 55° for $\psi = 0°$ down to 45° for $\psi = 90°$). The void ratio in the middle of the shear zone (Fig. 10a) approaches the pressure-dependent critical void ratio 0.76–0.80 (equation 24).The maximum strain measure in the shear zone changes between 2.01 ($\psi = 90°$) and 2.24($\psi = 0°$) at $u_2/h = 0.10$ (Fig. 10b). Both the shear zone thickness and the inclination change due to the varying peak internal friction angle and dilatancy angle (which both influence the shear zone inclination), and the varying stiffness in the softening regime (which influences the shear zone thickness). A comparison with the experimental results by Tatsuoka [48] (performed with a different specimen size and granular material) shows a satisfactory qualitative agreement with respect to the magnitude of the mobilized internal friction angle at peak and at residual state. However, the calculated vertical strain corresponding to the peak on the load-displacement curve does not change with the bedding plane orientation (Fig. 2).

During initial deformation, a pattern of shear zones can be first observed (Fig. 11). Next, strain localization continues to localize within a single zone which becomes visible at $u_2/h = 0.036$.

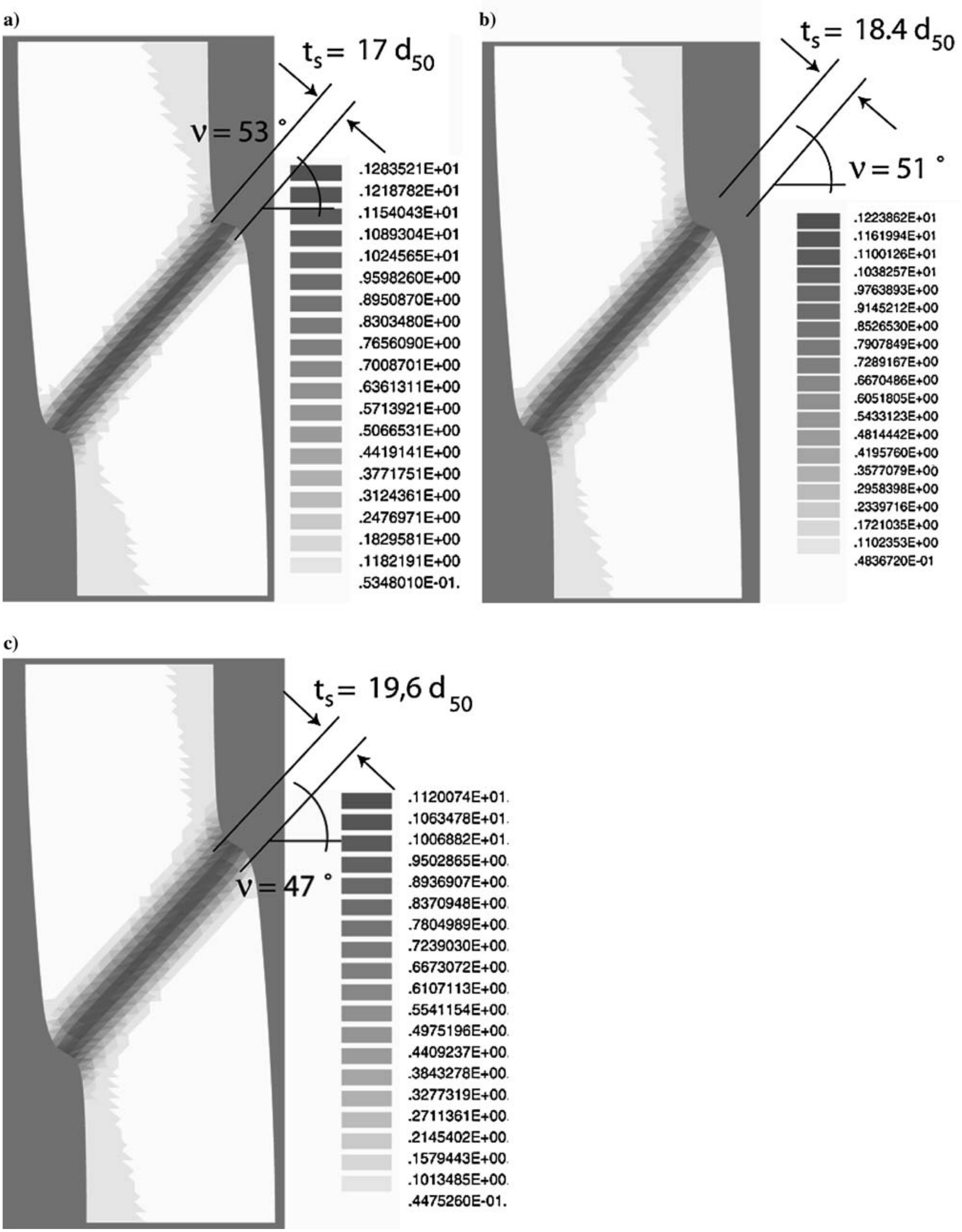

Fig. 13 Deformed specimen with the distribution of strain measure $\bar{\varepsilon} = \sqrt{\varepsilon_{ij}\varepsilon_{ij}}$ at residual state (uniform distribution of $e_0 = 0.60, d_{50} = 0.5$ mm, $\Delta e_{c0}(t = 0) = 0.25$, $B = 5$): **a** $\psi = 0°$, **b** $\psi = 45°$, **c** $\psi = 90°$

5.2 Uniform distribution of the initial void ratio

The normalized load-displacement curves for different bedding plane orientations θ with the initial uniform void ratio of $e_o = 0.60$ are shown in Fig. 12. No weak element was introduced to trigger shear localization. The deformed FE-mesh with the distribution of the strain measure $\bar{\varepsilon}$ before and after the peak, and at residual state is demonstrated in Figs. 13 and 14, respectively.

The vertical force on the top edge increases with decreasing bedding angle. All forces reach the same residual state. The shear strain corresponding to the maximum vertical force on the top is also similar. The peak internal friction angles lie between 38.1 and 42.2° (Fig. 13) and are slightly smaller than those calculated with a stochastic distribution of the initial void ratio (Fig. 9).

One shear zone occurs inside of the specimen although an uniform initial void ratio was assumed (Fig. 14). Its position is always the same in the specimen. The shear zone thickness slightly increases with increasing angle θ; from about $t_s = 8.5\,\text{mm}\ (17 \times d_{50})$ for $\psi = 0°$, $t_s = 9.2\,\text{mm}\ (18.4 \times d_{50})$ for $\psi = 45°$ up to $t_s = 9.8\,\text{mm}\ (19.6 \times d_{50})$ for $\psi = 90°$. In turn, the inclination against the bottom is about $\nu = 53°$ (for $\psi = 0°$), $\nu = 51°$ (for $\psi = 45°$) and $\nu = 47°$ (for $\psi = 90°$). Thus, the changes of the shear zone inclination are in agreement with tests [49].

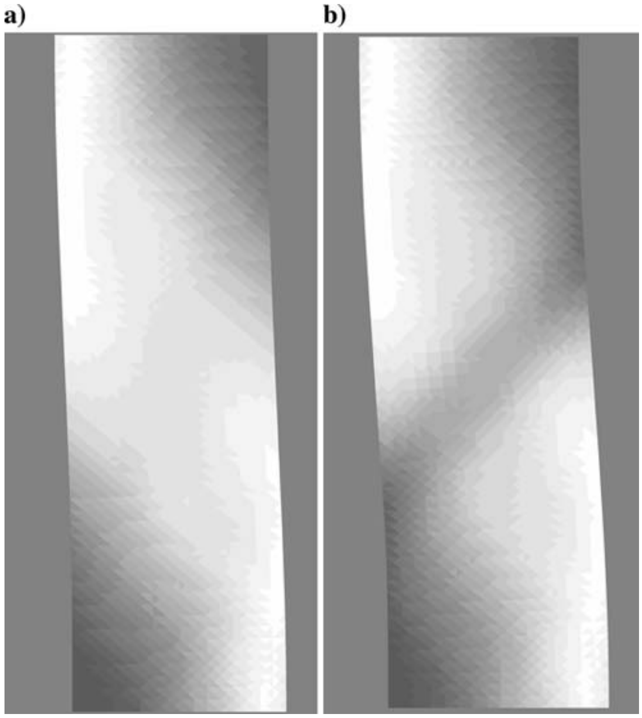

Fig. 14 Deformed specimen with distribution of strain measure $\bar{\varepsilon} = \sqrt{\varepsilon_{ij}\varepsilon_{ij}}$ at different vertical deformations: **a** $u_2/h = 0.045$, **b** $u_2/h = 0.054$ (uniform distribution of $e_0 = 0.60$, $d_{50} = 0.5\,\text{mm}$, $\Delta e_{c0}(t = 0) = 0.25$, $B = 5$, $\theta = 45°$)

The formation of shear localization is completely different in the initial phase (Fig. 14) as compared to the results with a stochastic distribution of the initial void ratio (Fig. 11). The shear localization initially develops simultaneously at the left low corner and at the right top corner. Next, an inclined shear zones occurs in the mid-region combining two regions which develops further reaching its final position.

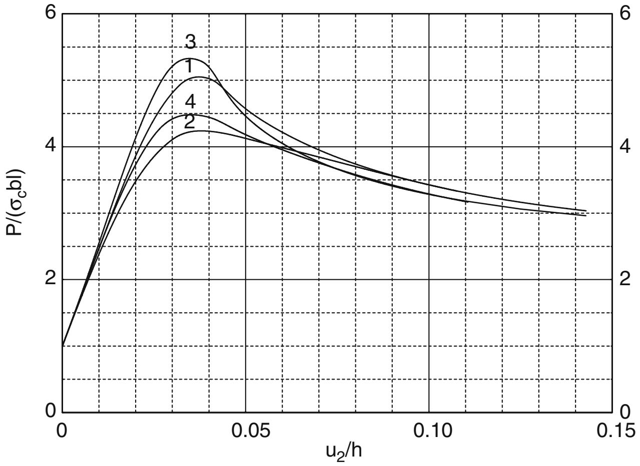

Fig. 15 Effect of the bedding plane inclination ψ of Fig. 6 on the normalized load-displacement curve ($d_{50} = 2\,\text{mm}$, $e_o = 0.60$, $\Delta e_{c0}(t = 0) = 0.25$, $B = 5$): 1 uniform distribution of e_o, $\psi = 0°$, 2 uniform distribution of e_o, $\psi = 90°$, 3 stochastic distribution of e_o, $\psi = 0°$, 4 stochastic distribution of e_o, $\psi = 90°$

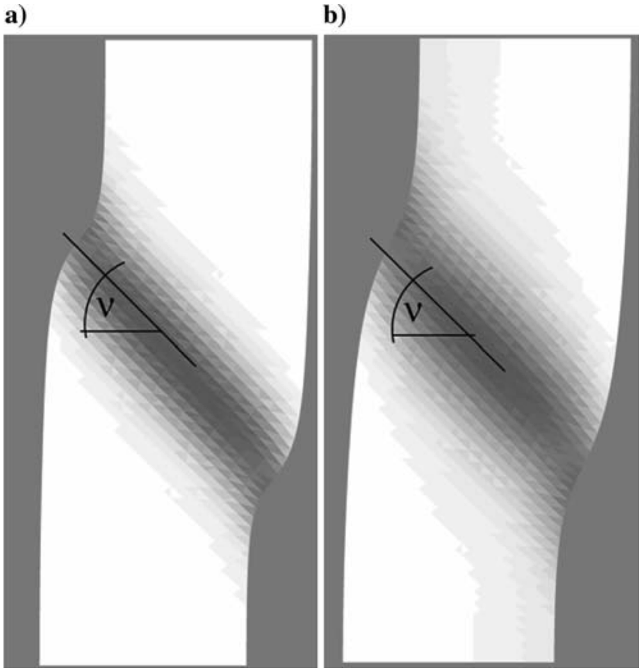

Fig. 16 Deformed specimen with the distribution of strain measure $\bar{\varepsilon} = \sqrt{\varepsilon_{ij}\varepsilon_{ij}}$ at residual state for uniform distribution of $e_o = 0.60$ ($d_{50} = 2.0\,\text{mm}$, $\Delta e_{c0}(t = 0) = 0.25$, $B = 5$): **a** $\psi = 0°$ ($t_s = 8.5 \times d_{50}$, $\nu = 48°$), **b** $\psi = 90°$ ($t_s = 10 \times d_{50}$, $\nu = 46°$)

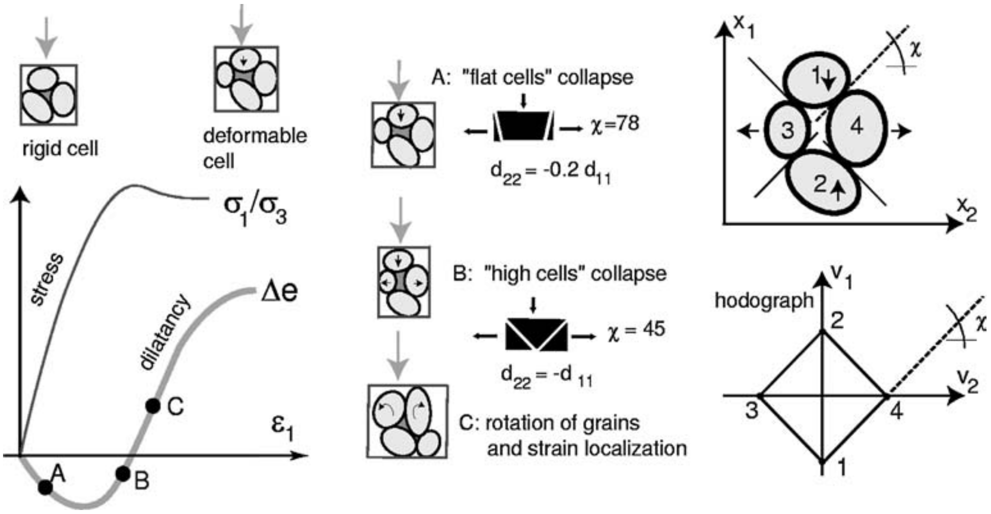

Fig. 17 Micromechanical 2-D interpretation of the dilatancy as a function of the average shape of deformable Voronoi cells in dense granulate for plane strain [62] : Voronoi cells consisting of three grains are considered rigid so only cells of four (or more) are of interest. A vertical compression (along x_1) causes that at first the flat cells collapse (*point A*). On continuing deformation (*point B*), due to the lack of flat cells also some square cells or high cells are being squeezed. This is happening at the expense of larger dilatancy and allows for higher stress ratios. The dilatancy resulting from the hodograph (velocity diagram for particles 1–4) depends on the angle χ of the contact normals. The zero average velocity of grains 1, 2, 3 and 4 is assumed. The inherent anisotropy expresses the dominant orientation of the flat cells

The effect of a larger characteristic length, $d_{50} = 2.0$ mm, on the shear zone formation is demonstrated in Figs. 15 and 16 using a stochastic and uniform distribution of $e_0 = 0.60$. The shear zone thickness is about 17 mm ($8.5 \times d_{50}$) for $\psi = 0°$ and 20 mm ($10 \times d_{50}$) for $\psi = 90°$ with the uniform distribution of e_0. The internal friction angles at peak are larger (stochastic distribution of e_0) and similar (uniform distribution of e_0) with the larger d_{50} as in the case of $d_{50} = 0.5$ mm. The material becomes more ductile after the peak [8].

6 Conclusions and discussion

The following conclusions can be derived from of FE-calculations of plane strain compression with a hypoplastic constitutive model enhanced by micro-polar terms to capture shear localization and by two additional parameters Δe_{c0} and B to describe textural anisotropy:

- The larger the bedding plane inclination ψ, the smaller the peak internal friction angle, Figs. 9 and 12 (similarly as in the experiments, Fig. 3). The physical interpretation of this effect is that the distribution of the grain contact normals has a preference towards the direction of sedimentation. Therefore the axial deformation in the direction of sedimentation causes additional dilatancy (implemented in the model via Δe_{c0}). This becomes clear from Fig. 17.
- The anisotropic effect vanishes at residual state Figs. 9 and 15 (similarly as in the experiments, Fig. 3). At large deformation anisotropy is erased because the position of grains and the shape of the Voronoi cells are significantly changed compared to the state directly after sedimentation (or pluviation).
- The shear zone thickness slightly increases with increasing bedding plane inclination ψ, Fig. 10. More detailed laboratory tests would be necessary to confirm this numerical finding.
- The shear zone inclination decreases (by about 5–10°) with increasing bedding plane inclination ψ (similarly as in the experiments [49]). It is caused by a decrease of the internal friction at peak and dilatancy angle with increasing ψ.
- In the case of the uniform distribution of the initial void ratio (without any imperfection), only a single shear zone occurs inside of the specimen (due to the lack of material re-hardening).
- The peak internal friction angles are larger when using the stochastic distribution of the initial void ratio (Fig. 9) as compared to the uniform distribution (Fig. 12). This effect is also observed in the case of spatially correlated fields of the void ratio [66]. It is caused by the fact that shear localization meets (on its straight propagation way through the specimen) intrusions in the form of elements with a different void ratio. Thus, the material shear resistance can be larger. Obviously, the weakest link principle does not apply here. The fact that the spatial fluctuation of the void ratio makes the material stronger indicates that the shear zone does not appear immediately throughout the whole specimen (in which case the weakest cross-section would be chosen) but that at the early stage of deformation, initially several shear zones propagate in the longitudinal starting from the weakest elements (Fig. 11).

7 Outlook

The FE-calculations will be continued for the 3D case and for water saturated fine-grained sand. A spatially correlated stochastic distribution of the initial void ratio will be developed according to [64,65]. The calculated void ratio changes will be checked with experiments using the Particle Image Velocimetry (PIV) technique [66].

8 Notation

Both matrix-vector and indexed tensorial notations are used. For summation of vector and matrix components, the Einstein's rule is applied. A superposed circle indicates objective time derivation and a superposed dot indicates material time derivation of a particular quantity. Compressive stress and shortening strain are taken as negative.

A	surface,
a_1	parameter representing the deviatoric part of the normalized stress in the critical state,
a_c	micro-polar constant,
b	specimen width,
B	material constant,
c_u	undrained cohesion,
C	material constant,
d	dilatancy,
d_{kl}	rate of deformation tensor (stretching tensor),
d^*_{kl}	deviatoric part of d_{kl},
d^c_{ij}	polar rate of deformation tensor,
d_{50}	mean grain diameter,
D	modulus of deformation rate,
e_o	initial void ratio,
e_c	critical void ratio,
e_d	void ratio at maximum densification,
e_i	maximum void ratio,
e_{c0}	value of e_c for σ_{kk}=0,
e_{d0}	value of e_d for σ_{kk}=0,
e_{i0}	value of e_i for σ_{kk}=0,
e	current void ratio,
E_{ijkl}	tangential stiffness,
f_{d}	density factor,
f_{s}	stiffness factor,
f^B_i	volume body forces,
h	initial height of the sand body,
h_s	granular hardness,
k_i	rate of curvature vector,
K_o	pressure coefficient at rest,
l	specimen length in the direction perpendicular to the deformation plane,
m_i	Cauchy couple stress vector,
$\overset{o}{m}_i$	Jaumann couple stress rate vector (objective couple stress rate vector),
m_1	horizontal couple stress,
m_2	vertical couple stress,
m^B	volume body moment,
n	compression coefficient,
p	Roscoe stress invariant ($p = 1/3(\sigma_1 + 2\sigma_2)$),
p_s	mean pressure,
P	resultant vertical force,
q	Roscoe stress invariant ($q = \sigma_1 \sigma_2$),
r	random number,
s_i	components of normal unit vector of the bedding plane,
t	time,
t_s	shear zone thickness,
u_2	vertical displacement of the top boundary,
w_{ij}	spin tensor,
w^c	rate of Cosserat rotation,
v	material velocity,
V	volume
x_2	vertical coordinate measured from the top of the specimen,
α	pycnotropy coefficient,
β	stiffness coefficient,
δ	angle of the direction of the major principal stress relative to the bedding plane direction,
γ_d	initial volume weight,
γ	shear strain,
ϕ_c	critical angle of internal friction during stationary flow,
ϕ_m	mobilized angle of internal friction,
$\bar{\varepsilon}$	strain measure ($\bar{\varepsilon} = \sqrt{\varepsilon_{ij}\varepsilon_{ij}}$),
ε_i	principal strains,
ε_{11}	vertical horizontal strain,
ε_{22}	vertical normal strain,
ε_{12}	horizontal shear strain,
ε_{21}	vertical shear strain,
ε_v	volumetric strain ($\varepsilon_v = \varepsilon_1 + 2\varepsilon_2$),
ε_i	principal strains,
ε_q	strain measure ($\varepsilon_q = \varepsilon_1 - \varepsilon_2$),
χ	angle of the contact normals,
ν	shear zone inclination against the bottom,
σ_{ij}	Cauchy stress tensor,
σ_i	principal stresses,
σ^*_{ij}	deviatoric part of σ_{ij},
$\overset{o}{\sigma}_{ij}$	Zaremba-Jaumann stress rate tensor (objective stress rate tensor),
$\overset{o*}{\sigma}_{ij}$	deviatoric part of Zaremba-Jaumann stress rate tensor,
σ_{11}	horizontal normal stress,
σ_{22}	vertical normal stress,
σ_{33}	horizontal normal stress perpendicular to the deformation plane,
σ_{12}	horizontal shear stress,
σ_{21}	vertical shear stress,
σ_{conf}	confining pressure,
θ	Lode angle,
ψ	bedding angle,
ω^c	Cosserat rotation.

References

1. Kolymbas, D.: A rate-dependent constitutive equation for soils. Mech. Res. Comm., **6**, 367–372 (1977)
2. Wu, W.: Hypoplastizität als mathematisches Modell zum mechanischen Verhalten granularer Stoffe. Publication Series of the Institute of Soil and Rock Mechanics, University Karlsruhe, 129, (1992)

3. Gudehus, G.: A comprehensive constitutive equation for granular materials. Soils Foundations **36**(1), 1–12 (1996)
4. Bauer, E.: Calibration of a comprehensive hypoplastic model for granular materials. Soils Foundations **36**(1), 13–26 (1996)
5. von Wolffersdorff, P. A.: A hypoplastic relation for granular materials with a predefined limit state surface. Mech. Cohesive-Frictional Mater. **1**, 251–271 (1996)
6. Niemunis, A.: Extended hypoplastic models for soils. *Habilitation Monography*. Gdansk University of Technology (2003)
7. Maier, T.: Numerische Modellierung der Entfestigung im Rahmen der Hypoplastizität. *PhD Thesis*, University of Dortmund (2002)
8. Tejchman, J.: Influence of a characteristic length on shear zone thickness in hypoplasticity with different enhancements. Comput. Geotech. **31**(8), 595–611 (2004)
9. Boehler, J.P., Sawczuk, A.: On yielding of oriented solids. Acta Mech. **27**, 185–206 (1977)
10. Kanatani, K.I.: Distribution of directional data and fabric tensor. Int. J. Eng. Sci. **22**, 149–160 (1984)
11. Oda, M., Nemat-Nasser, Konishi, J.: Stress induced anisotropy in granular masses. Soils Foundations **25**(3), 85–97 (1985)
12. Satake, M.: A theory on the stress-induced anisotropy. In: Garcia-Rojo, Herrmann, McNamara (eds.), Powders and grains, Taylor and Francis Group, London, pp. 155–158 (2005)
13. Khidas, Y., Jia, X.: Acoustic measurements of anisotropic elasticity in glass beads packings. In: Garcia-Rojo, Herrmann, McNamara (eds.), Powders and grains, Taylor and Francis Group, London, pp. 309–312 (2005)
14. Kuhn, M.R.: Scaling in granular materials. In: Garcia-Rojo, Herrmann, McNamara (eds.), Powders and grains, Taylor and Francis Group, London, pp. 115–122 (2005)
15. Dafalias, Y.F., Papadimitriou, A., G., Xiang, X.S.: Sand plasticity model accounting for inherent fabric anisotropy. J. Eng. Mech. ASCE. **130**, 1319–1333 (2004)
16. Tatsuoka, F.: Impacts on geotechnical engineering of several recent findings from laboratory stress-strain tests on geomaterials. Lecture note for the 2000 Burmister Lecture, October 2000, Columbia University (2000)
17. Han, C., Vardoulakis, I.: Plane strain compression experiments on water saturated fine-grained sand. Geotechnique **41**, 49–78 (1991)
18. Rowe, P.W.: The stress-dilatancy relation for static equilibrium of an assembly of particles in contact. Proc. R. Soc. Lond. A **269**, 500–527 (1962)
19. Doanh, T., Finge, Z., Boucq, S., Dubujet Ph.: Historiotropy of Hostun RF loose sand. Proceedings of the Conference "Modern Trends in Geomechanics". Springer, Vienna (2006) (In press)
20. Pena, A.A., Herrmann, H.J., Lizcano, A., Alonso-Marroquin, F.: Investigation of the asymptotic states of granular materials using a discrete model of anisotropic particles. In: Garcia-Rojo, Herrmann, McNamara (ed.), Powders and Grains, Taylor and Francis Group, London, pp. 697–700 (2005)
21. Schoffield, A.N., Wroth, C.P.: Critical State Soil Mechanics. Mc Graw Hill, London (1968)
22. Desrues, J., Chambon, R., Mokni, M., Mazerolle, F.: Void ratio evolution inside shear bands in triaxial sand specimens studied by computed tomography. Geotechnique **46**, 529–546 (1996)
23. Vermeer, P.: A five-constant model unifying well-established concepts. In:Gudehus, G., Darve, F., Vardoulakis, I. (ed.), Proceedings of international workshop on constitutive relations for soils. Balkema, pp. 175–197 (1982)
24. Lade, P.V.: Elasto-plastic stress-strain theory for cohesionless soil with curved yield surfaces. Int. J. Solid Struct. **13**, 1019–1035 (1977)
25. Pestana, J.M., Whittle, A.J.: Formulation of a unified constitutive model for clays and sands. In. J. Num. Anal. Meth. Geomech. **23**, 1215–1243 (1999)
26. Desrues, J., Chambon, R.: Shear band analysis for granular materials – the question of incremental linearity. Ingenieur Arch **59**, 187–196 (1989)
27. Darve, F., Flavigny, E., Megachou, M.: Yield surfaces and principle of superposition revisited by incrementally non-linear constitutive relations. Int. J. Plasticity **11**(8), 927–948 (1995)
28. Lanier, J., Caillerie, D., Chambon, R.: A general formulation of hypoplasticity. Int. J. Numer. Anal. Methods in Geomech. **28**(15), 1461–1478 (2004)
29. Mühlhaus, H.-B.: Continuum models for layered and blocky rock. In: Hudson, J.A., Fairhurst, Ch. (eds.), Comprehensive rock engineering, vol. 2, pp. 209–231. Pergamon Press, Newyork (1990)
30. Tejchman, J., Wu, W.: Numerical study on shear band patterning in a Cosserat continuum. Acta Mech. **99**, 61–74 (1993)
31. Tejchman, J., Gudehus, G.: Shearing of a narrow granular strip with polar quantities. J. Num. Anal. Methods Geomech. **25**, 1–18 (2001)
32. Huang, W., Nübel, K., Bauer, E.: A polar extension of hypoplastic model for granular material with shear localization. Mech. Mater. **34**, 563–576 (2002)
33. Gudehus, G., Nübel, K.: Evolution of shear bands in sand. Geotechnique **54**(3), 187–201 (2004)
34. Bažant, Z., Lin, F., Pijaudier-Cabot, G.: Yield limit degradation: non-local continuum model with local strain. In: Owen (ed.), Proceedings of international conference computational plasticity, Barcelona, pp. 1757–1780 (1987)
35. Brinkgreve, R.: Geomaterial models and numerical analysis of softening. Dissertation, Delft University, pp. 1–153 (1994)
36. Aifantis, E.C.: On the microstructural origin of certain inelastic models. J. Eng. Mater. Technol. **106**, 326–334 (1984)
37. de Borst, R., Mühlhaus, H.-B.: Gradient dependent plasticity: formulation and algorithmic aspects. Int. J. Numer. Methods Eng. **35**, 521–539 (1992)
38. Pamin, J.: Gradient-dependent plasticity in numerical simulation of localisation phenomena. PhD Thesis, Delft University, pp. 1–134 (1994)
39. Loret B., Prevost, J.H.: Dynamic strain localisation in elasto-visco-plastic solids, Part 1. General formulation and one-dimensional examples. Comp. Appl. Mech. Eng. **83**, 247–273 (1990)
40. Sluys, L.J., de Borst, R.: Dispersive properties of gradient and rate-dependent media. Mech. Mater. **183**, 131–149 (1994)
41. de Borst, R., Mühlhaus, H.-B., Pamin, J., Sluys, L.: Computational modelling of localization of deformation. In: Owen, D.R.J., Onate, H., Hinton, E. (eds.), Proceedings of the 3rd International Conference Computational Plasticity, Swansea, Pineridge Press, pp. 483–508 (1992)
42. Larsson, J., Larsson, R.: Finite-element analysis of localization of deformation and fluid pressure in elastoplastic porous medium. Int. J. Solids and Structures **37**, 7231–7257 (2000)
43. Simone, A., Sluys, L.: Continous-discountinous modeling of mode-I and mode-II failure. In: Vermeer, P.A., Ehlers, W., Herrmann, H.J., Ramm E. (ed.), Modelling of cohesive-frictional materials, Balkema, pp. 323–337 (2004)
44. Tatsuoka, F., Goto, S., Tanaka, T., Tani, K., Kimura, Y.: Particle size effects on bearing capacity of footing on granular material. In: Asaoka, A., Adachi, T., Oka, F. (ed.), Deformation and Progressive Failure in Geomechanics Pergamon, pp. 133–138 (1997)
45. Arthur, J.R.F., Phillips, A.B.: Homogeneous and layered sand in triaxial compression. Geotechnique **25**(4), 799–815 (1975)
46. Lam, W.K., Tatsuoka, F.: Effect of initial anisotropic fabric and on strength and deformation characteristics of sand. Soils Foundations **28**(1), 89–106 (1988)
47. Tatsuoka, F., Nakamura, S., Huang, C., Tani, K.: Strength anisotropy and shear band direction in plane strain tests of sand. Soils Foundations **30**(1), 35–54 (1990)
48. Tatsuoka, F., Siddiquee, M.S.A., Yoshida, T., Park, C.S., Kamegai, Y., Goto, S., Kohata, Y.: Testing methods and results of element tests and testing conditions of plane strain model bearing capacity tests using air-dried dense Silver Leighton Buzzard sand. Internal Report of the Tokyo University, pp. 1–120, (1994)
49. Abelev, A.V., Lade, P.V.: Effects of cross anisotropy on 3-dimensional behaviour of sand. II: Stress-strain behaviour and shear banding. J. Eng. Mech. ASCE. **129**(2), 167–174 (2003)
50. Yamada, Y., Ishihara, K.: Anisotropic deformation characteristics of sand under three dimensional stress conditions. Soils Foundations **19**(2), 79–94 (1979)

51. Bauer, E., Huang, W., Wu, W.: Investigations of shear banding in an anisotropic hypoplastic material. Int. J. Solids Struct. **41**, 5903–5919 (2004)
52. Wu, W.: Rational approach to anisotropy of sand. Int. J. Numer. Anal. Meths. Geomech. **22**, 921–940 (1998)
53. Niemunis, A.: Anisotropic effects in hypoplasticity. In: Proceedings of international symposium on deformation characteristics of geomaterials, Vol 1, pp. 1211–1217, Lyon, France, (2003a) Geomech. **4**, 103–119 (1980)
54. Oda, M., Konishi, J., Nemat-Nasser, S.: Experimental micromechanical evaluation of strength of granular materials, effects of particle rolling. Mechanics of Mater., **1**, 269–283 (1982)
55. Oda, M.: Micro-fabric and couple stress in shear bands of granular materials. In: Thornton, C. (ed.), Powders and Grains, Rotterdam, Balkema, pp. 161–167 (1993)
56. Tejchman, J.: Shearing of an infinite narrow granular layer between two boundaries. In: Mühlhaus, H.B., et al., (eds.) Bifurcation and Localisation Theory in Geomechanics, Swets and Zeitlinger, Lisse, pp. 95–102 (2001)
57. Pasternak, E., Mühlhaus, H.-B.: Cosserat continuum modelling of granulate materials. In: Valliappan, S., Khalili, N. (ed.), Computational Mechanics – New Frontiers for New Millennium, Elsevier Science, Amsterdam, pp. 1189–1194 (2001)
58. Herle, I., Gudehus, G.: Determination of parameters of a hypoplastic constitutive model from properties of grain assemblies. Mech. Cohesive Frictional Mater. **4**(5), 461–486 (1999)
59. Vardoulakis. I.: Shear band inclination and shear modulus in biaxial tests. Int. J. Num. Anal. Meth. Geomech. **4**, 103–119 (1980)
60. Shahinpoor, M.: Statistical mechanical considerations on storing bulk solids. Bulk Solid Handling **1**(1), 31–36 (1981)
61. Nübel, K., Karcher, C.: FE simulations of granular material with a given frequency distribution of voids as initial condition. Granular Matter **1**(3), 105–112 (1998)
62. Niemunis, A.: Bodenmechanik 2, Script, University of Bochum http://www.ruhr-uni-bochum.de/gub/mitarbeiter/andrzej_niemunis.htm, 2004.
63. Tejchman, J.: FE-analysis of shear localization in 2-D random granular bodies. In: Proceedings of International Conference of ICCS 2006, Reading, Great Britain (2006)
64. Walukiewicz, H., Bielewicz, E., Gorski, J.: Simulation of nonhomegeneous random fields for structural applications. Comput. Struct. **64**(1–4), 491–498 (1997)
65. Tejchman, J.: Effect of fluctuation of current void ratio on the shear zone formation in granular bodies within micro-polar hypoplasticity. Comput. Geotech (2006) (In press)
66. Slominski, C., Niedostatkiewicz, M., Tejchman, J.: Deformation measurements in granular bodies using a particie image velocimetry technique. Archiv. Hydro-Eng. Environ. Mech. Polish Acad. Sci. (2006) (In press)